Published in final edited form as:
NMR Biomed. 2010 December ; 23(10): 1127–1136. doi:10.1002/nbm.1539.

Improved R2* Measurement Accuracy with Absolute SNR Truncation and Optimal Coil Combination

Xiaoming Yin, MS[1,2], **Saurabh Shah, MS**[4], **Aggelos K. Katsaggelos, Ph.D**[2], and **Andrew C. Larson, Ph.D**[1,2,3]

[1]Department of Radiology, Northwestern University, Chicago, IL, USA

[2]Department of Electrical Engineering and Computer Science, Northwestern University, Chicago, IL, USA

[3]Robert H. Lurie Comprehensive Cancer Center, Northwestern University, Chicago, IL, USA

[4]Siemens Medical Solutions, MR Research and Development, Chicago, Illinois, USA

Abstract

Accurate R2* measurements are critical for many abdominal imaging applications. Conventionally, R2* maps are derived via mono-exponential fitting of signal decay within a series of gradient echo (GRE) images reconstructed from multi-channel datasets combined using a root sum-of-squares (RSS) approach. However, the noise bias at low SNR TEs from RSS reconstructed data often causes underestimation of R2* values. In phantom, ex *vivo* animal model, and normal volunteer studies, we investigated the accuracy of low SNR R2* measurement when combining truncation and coil combination methods. The accuracy for R2* estimations was shown to be affected by the intrinsic R2* value, SNR level, and chosen reconstruction method. R2* estimation error was found to decrease with increasing SNR level, decreasing R2* value, and use of the optimal B1-weighted combined (OBC) image reconstruction method. Data truncation based upon rigorous voxel-wise SNR estimates can reduce R2* measurement error in the setting of low SNR with fast signal decay. When optimal SNR truncation thresholds are unknown, the OBC method can provide optimal R2* measurements given the minimal truncation requirements.

Keywords

multiple gradient echo; R2* mapping; truncation; signal to noise ratio; optimal B1-weighted image reconstruction; root sum-of-square; phase array coils; noise bias

Introduction

Accurate R2* measurements are critical for an increasing number of abdominal imaging applications (1,2,3,4). Typically, R2* is estimated via mono-exponential fitting of signal decay within a series of gradient echo (GRE) images sampled at increasing echo times (TEs). For a single receiver channel, signal within a magnitude image resembles a Rician distribution due to the presence of noise (5). However, the signal distribution for multi-channel datasets depends upon the chosen reconstruction and channel-combination technique. For conventional R2*-mapping methods, images reconstructed from multi-channel datasets are combined using a root sum-of-squares (RSS) approach (1,2,4). For RSS

The corresponding author: Andrew C. Larson, Northwestern University, Department of Radiology, 737 North Michigan Ave. 16th Floor, Chicago, IL, 60611, Tel: (312) 926-3499 Fax: (312)926-5991, a-larson@northwestern.edu.

images at shorter TE with higher signal-to-noise ratio (SNR), signal magnitudes can be approximated by Gaussian distributions. However, as the signal decays, resulting in lower SNR at later echoes, the noisy signal begins to resemble non-central chi-distributions (6). These non-central chi-distributions can result in systematic noise bias and underestimation of R2* values (7).

Recent development efforts have focused upon two general approaches to improve R2* measurement accuracy: 1) data correction and 2) SNR improvement. Data correction methods are applied to magnitude data prior to mono-exponential fitting. Commonly used approaches include: noise correction, baseline subtraction, offset addition, and truncation (8,9,10,11). Proposed noise correction methods involve fitting the power signal after subtraction of background noise power rather than simply fitting the magnitude decay signal (8,12). Baseline subtraction methods subtract the mean background noise from each image prior to the mono-exponential fitting process (13,14). Offset models have been proposed to account for noise effects when estimating the mono-exponential decay component by adding a constant offset value to the fitted data model (10), however, these may lead to an overestimation of R2* values (11). Empirical data truncation is the most commonly used method to avoid noise bias during R2* measurements. This method involves simply truncating the signal decay curve and fitting only those signals sampled at earlier TEs prior to the signal descending below the noise floor (1,2,15,16). Recently, He *et al.* (1) compared noise-corrected data to originally acquired data and found that the T2* measurements from corrected data were more accurate; truncation methods were determined to be the most accurate and reproducible.

Truncation models require accurate SNR estimates for each voxel at each TE to either include or exclude a data point during the mono-exponential fitting process. For RSS reconstruction schemes, SNR estimates can be derived by measuring noise within a background region. Noise can also be estimated using noise-only pre-scans and RSS images can be reconstructed in SNR units (17). Alternatively, B1-weighted reconstruction schemes (18,19) can be employed to provide superior SNR and improve signal fidelity at later TEs. Previous studies have demonstrated that optimal B1-weighted image reconstruction provides superior accuracy during low SNR T2 and T2* measurements when compared to RSS reconstruction methods (7). Improved multi-channel combination methods were also found to provide superior accuracy during estimation of mono-exponential decay diffusion coefficients for DTI (20).

There remains uncertainty as to which of the aforementioned approaches is optimal for abdominal R2* mapping. The objective of our work was to investigate the accuracy of each approach during low SNR R2* measurements (common for visceral organs located relatively far from the abdominal surface coil array). Multi-echo multi-coil datasets were reconstructed using both RSS and optimal B1-weighted combined (OBC) methods, voxel-wise SNR estimates were calculated using above mentioned approaches and R2* maps were derived using truncation model with mono-exponential fit. We compared the accuracy of these methods in phantoms, an *ex vivo* animal model, and healthy volunteers.

Materials and Methods

R2* Quantification Methods

We utilized a previously described truncation method (1) which involves selecting only those signals above an SNR threshold for mono-exponential fitting of R2* signal decay (signals collected at later TEs below SNR threshold were excluded). Following methods were utilized to estimate or rigorously calculate SNR within individual images.

1. *Method A – GlobalRSS:* For this method we used a common, straightforward approach to estimate SNR within each image (21,22). First, images at each TE were reconstructed using the RSS approach. Next, a region-of-interest (ROI) was drawn to calculate the standard deviation (σ_{BG}) of the background noise within each image. Voxel-wise $SNR_{GlobalRSS}$ was then calculated within each image as the ratio between signal intensity (SI) and σ_{BG} multiplied by a correction factor, Equ [1a], where N is the number of coils used and β(N) can be calculated from Equ [1b]. For R2* measurements, all TE with $SNR_{GlobalRSS}$ below a given threshold were excluded from R2* map calculations. R2* maps were calculated via voxel-wise non-linear least-square fitting of the mono-exponential signal decay. A minimum of two TEs were kept for all R2* estimations (even if both fell bellow the respective SNR truncation threshold). We refer to *Method A* as the *GlobalRSS* approach given that a global noise estimate is utilized during all subsequent SNR calculations.

$$SNR_{GlobalRSS} = \frac{SI}{\sqrt{2N - \beta(N)^2 \sigma_{BG}}} \quad [1a]$$

$$\beta(N) = \sqrt{\frac{\pi}{2}} \frac{(2N-1)!!}{2^{N-1}(N-1)!} \quad [1b]$$

2. *Method B - VoxelRSS:* For this method, we reconstructed all images in rigorously calibrated SNR units using RSS approach for multi-channel data combination (17). First, large samples of noise-only pre-scans (12288 noise samples) were performed to estimate coil dependent noise characteristics and calculate a noise covariance matrix, R_n. At each TE, images were produced in absolute SNR units ($SNR_{VoxelRSS}$) via combination of the complex images from each channel according to Equ [2] where p is the vector of complex signal values from each coil and H is the Hermitian operator. The calculated $SNR_{VoxelRSS}$ value for each voxel was also corrected for inherent noise bias. This was accomplished by subtraction of a correction factor that was dependent upon the total number of channels used to collect the data (17,23). For R2* measurements, all TEs with $SNR_{VoxelRSS}$ below a chosen threshold were excluded from R2* map calculations.

$$SNR_{VoxelRSS} = \sqrt{2\, p^H R_n^{-1} p} \quad [2]$$

Method C - VoxelOBC: For this method, we again reconstructed all images in rigorously calibrated SNR units but used the OBC approach for multi-channel data combination (17). We estimated coil sensitivity maps based upon images collected for each channel at the shortest TE. At each pixel of the image, we computed a covariance matrix and then obtained the optimal estimate of the coil sensitivity by finding the eigenvector of the covariance matrix (24). A noise covariance matrix, R_n, was calculated from the noise-only pre-scans. At each TE, images were produced in absolute SNR units ($SNR_{VoxelOBC}$), Equ [3], with b the complex coil sensitivity profiles. SNR corrections were performed to remove noise bias (17). For R2* measurements, all TE with $SNR_{VoxelOBC}$ below a given threshold were excluded from R2* map calculations.

$$SNR_{VoxelOBC} = \frac{\sqrt{2}\left|b^H R_n^{-1} p\right|}{\sqrt{b^H R_n^{-1} b}} \quad [3]$$

Phantom Studies

Cylindrical 2L polystyrene bottles were filled with water and doped with 1.6, 1.2, or 0.8mmol/L $MnCl_2.H_2O$ (*Phantoms I, II, and III*) to produce a wide range of R2* values. Phantom studies were performed using a 3T clinical scanner (MAGNETOM Trio, Siemens AG HCS, Erlangen, Germany) with an 8-channel head receiver coil. The Trio scanner had a horizontal bore with 60cm inner diameter. Its gradient system offered a maximum amplitude of 45 mT/m along each axis and maximum slew rate of 200 T/m/s. Phantoms were positioned such that the 8 coil-profiles were unevenly distributed about the circumference of each bottle. For data acquisition, a conventional multi-gradientecho (MGRE) sequence was used with parameters listed in Table 1. Data were acquired such that multiple echoes were generated following a single RF excitation. We achieved a wider range of SNR levels by sampling MGRE datasets using different flip-angles (FA)=1°, 2°, and 5°. For reference standard R2* measurements, we acquired high SNR datasets using a separate acquisition with the following parameters: body transmitter/receiver coil for excitation/reception, 32 averages, TR=5000ms, and FA=90°. We used a large flip angle to maximize SNR while an extended sequence TR to limit T1 weighting and saturation effects.

Animal Model Studies

Abdominal axial MGRE scans were performed in a recently euthanized New Zealand White rabbit. This animal was part of a separate ACUC approved hind-limb tumor model study. These *ex vivo* studies were performed to examine the accuracy of the proposed R2* methods while avoiding breath-holding complications. The animal model study was performed using the aforementioned 3T clinical scanner and 8-channel head coil (see Table 1 for sequence parameters). Reference standard R2* measurements from high SNR data were performed using the body transmitter/receiver coil (32 averages, TR=5000ms, FA=90°). We separately evaluated R2* measurement accuracy within the liver and gallbladder, which exhibit short and long transverse relaxation times, respectively.

Volunteer Studies

Abdominal axial MGRE scans were performed in 6 healthy volunteers in accordance with our IRB-approved protocol. Volunteer studies were conducted using a 1.5T clinical scanner (MAGNETOM Avanto, Siemens AG HCS, Erlangen, Germany) and a 32-channel surface receiver coil array. The Avanto scanner had a horizontal bore with 60cm inner diameter. Avanto gradient system has maximum amplitude of 45 mT/m and maximum slew rate of 200 T/m/s. Sequence parameters were chosen to permit acquisition of R2*-weighted images across a wide range of TEs within a single breath-hold (Table 1). Normal volunteer studies lacked a “reference standard” acquisition due to the limitation on breath-hold time and the complication of misregistration of the images acquired at different breath-hold positions.

Data Analysis

For phantom and animal model studies, we computed mean voxel-wise absolute error (VAE) between the reference-standard R2* map derived from high SNR data, $R2^*_{High\ SNR}$, and the reconstructed R2* maps, $R2^*_R$ (derived using *Methods A*, *B*, and *C*) according to Equ [4], where *k* is the image voxel index. For phantom studies, VAE measurements included only voxels within a circular ROI contained within the phantom boundary. For animal model study, separate ROIs were drawn within the liver and gallbladder excluding

blood vessels. Mean VAE was evaluated for each model at SNR truncation thresholds incremented from SNR=0 to 20(steps of 0.1 SNR units).

$$\text{Mean VAE}=\frac{\left|\sum_k R2^*_{HighSNR} - R2^*_R\right|}{\sum_k} \quad [4]$$

For volunteer studies, we first reconstructed R2*maps using *Methods A*, *B*, and *C* at SNR truncation thresholds from SNR=0 to 20 (steps of 0.1 SNR units). However, we lacked a "reference-standard" for absolute comparison of R2* measurement accuracy. Alternatively, we performed comparisons between the R2* values measured for each volunteer using each of the three *Methods* (*A*, *B*, and *C*). These comparisons were performed separately for a) an ROI within a peripheral, relatively high SNR region in the liver near the chest array coil and b) a centrally located ROI in the liver with lower SNR. For both ROIs, these comparisons were repeated for R2* measurements at four representative SNR truncation thresholds (0, 7, 14, and 20). We used ANOVA multiple comparison tests with Tukey post-hoc analyses (α=0.05) to determine any statistically significant differences between the methods.

Results

Phantom Results

Our phantom experiments demonstrated the differential impact of noise and R2* signal decay upon the accuracy of subsequent R2* estimates. *Phantom I* and *Phantom III* images for FA=2° (relatively low SNR) at TE=1.51ms, 13.36ms, 27.58ms, 56.02ms (echoes 1, 6, 12, and 24) are shown in Fig.1a. The R2* value for *Phantom I* was much greater than the R2* value for *Phantom III* (R2*=155 s^{-1} vs. R2*=80 s^{-1} for high SNR data measurement); signal within *Phantom I* images decayed more rapidly to the noise floor. For both phantoms at later TEs, OBC images demonstrated decreased noise levels compared to RSS images. Representative ROI drawn for comparisons of signal intensities and SNR measurements is shown within the RSS reconstructed image at TE=1 in Fig.1a. Mean signal decay within RSS, OBC, and high SNR data (reference standard) *Phantom I* and *Phantom III* image series are shown in Fig.1b (signals were normalized for display purposes). The impact of noise bias resulting from RSS reconstruction is clearly demonstrated within these plots; RSS signal decays more rapidly to its noise floor than OBC reconstructed images signal. If signal at all TEs for each dataset are used to estimate R2* values (i.e., no truncation), this noise bias can lead to significant R2* estimation inaccuracies. SNR measurements at all TEs for each of the reconstruction methods are shown in Fig.1c. Noise bias had a stronger impact upon SNR measurements for RSS reconstructed data ($SNR_{GlobalRSS}$ and $SNR_{VoxelRSS}$) than OBC reconstructed data ($SNR_{VoxelOBC}$). SNR measurements for OBC and RSS reconstruction methods were similar over a wider range of early TEs for *Phantom III* due to slower signal decay (shorter R2* compared to *Phantom I*). *Phantom II* (high SNR data R2*=100 s^{-1}) images and signal plots are omitted for brevity but represented a progression between corresponding results from *Phantoms I* and *III* having longer and shorter R2* values, respectively.

For FA=1°, 2°, and 5°, mean VAE at truncation thresholds from 0 to 20 are displayed in Fig. 2 for each of the three R2* phantoms. As demonstrated, given the same echo time range, mean VAE reduced with increasing SNR (increased FA) and decreasing R2* value (*Phantom I* to *Phantom III*). Mean VAE curves typically approached their minimum value as the SNR truncation threshold was decreased; mean VAE increased with the use of

increasingly higher truncation thresholds. At lower SNR thresholds, the mean VAE of the three methods were far apart but converged to similar levels once using higher SNR truncation thresholds. In general, *Method C* (*VoxelOBC*) achieved the minimum VAE level with little need for truncation of lower SNR data (FA=1° and FA=2°) and no need for truncation of higher SNR data (FA=5°). In contrast, *Method A* (*GlobalRSS*) and *Method B* (*VoxelRSS*) each required data truncation even at higher SNR thresholds to achieve optimum accuracy. Among the three methods, *Method C* (*VoxelOBC*) had the lowest minimum VAE and *Method A* (*GlobalRSS*) had the highest.

Animal Model Results

Similar to our phantom experiments, animal experiments also clearly demonstrated the impact of noise on R2* estimates. Axial abdominal images for FA=2° at TE=1.51ms, 13.36ms, 27.58ms, 56.02ms (echoes 1, 6, 12, and 24) are shown in Fig.3a. Representative liver and gallbladder ROIs are shown within RSS reconstructed images at TE=1.51ms (RA and RB, respectively) in Fig.3a. At later TEs, RSS reconstructed images appeared much noisier than OBC images. Our reference standard R2* value for the rabbit liver (measured using the high SNR data) was greater than the R2* value for the gallbladder (R2*=160 s^{-1} vs. R2*=50 s^{-1}); mean liver signal decayed to the noise floor at a faster rate. Note however that the *ex vivo* measured R2* values for liver and gallbladder were greater than the R2* values typically anticipated for normal *in vivo* tissues (for example: R2* values for normal rabbit liver tissue were measured to be ≈ 30-50 s^{-1} in (26) likely due to the accumulated deoxyhemoglobin and/or temperature reductions post-euthanization (25,26). Normalized mean signal intensity plots for liver (RA) and gallbladder (RB) within RSS, OBC, and high SNR data reconstructions are shown in Fig.3b. Noise bias exerted a greater impact upon RSS reconstructions than OBC reconstructions. SNR measurements for both tissues are shown in Fig.3c. For liver tissue at later TEs, $SNR_{GlobalRSS}$ was shown to be greater than $SNR_{VoxelRSS}$ and $SNR_{VoxelOBC}$ due to noise bias. For gallbladder tissues, SNR measurements from both of the reconstruction methods appeared similar over the sampled range of TEs due to slower signal decay (reduced R2* compared to liver).

For FA=1°, 2°, and 5°, mean VAE for liver parenchyma and gallbladder tissue at truncation thresholds from 0 to 20 are shown in Fig.4. Similar to phantom results, mean VAE was reduced with increasing SNR (increased FA) and decreasing R2* value (liver vs. gallbladder) given the same echo time range. Mean VAE curves approached their minimum as the SNR truncation threshold was decreased; mean VAE increased with the use of increasingly higher truncation thresholds. To achieve minimum mean VAE level, *Method C* (*VoxelOBC*) required limited truncation of the data while *Method A* (*GlobalRSS*) and *Method B* (*VoxelRSS*) required data truncation at higher SNR thresholds. At low SNR thresholds, the three methods were at quite different VAE levels. These differences were reduced to a minimum at higher SNR thresholds and later converged. At all SNR levels for both liver and gallbladder R2* measurements, *Method C* (*VoxelOBC*) produced the lowest minimum VAE and *Method A* (*GlobalRSS*) produced the highest VAE.

Volunteer Results

For a representative volunteer at FA=20°, abdominal R2* maps are shown in Fig.5a derived from 24 TEs of RSS and OBC reconstructed images. For R2* map reconstructed from RSS method, the measured R2* values for liver parenchyma were higher (≈48 s^{-1}) in the peripheral region of the liver closer to the surface coil receivers and lower (≈27 s^{-1}) in the deep visceral tissue further away from the surface coil receivers. However, for the R2* map derived using OBC method, a similar range of R2* values were measured throughout the liver parenchyma (≈55 s^{-1}-61 s^{-1}), independent of tissue depth relative to coil position. For each volunteer, we selected separate ROI in the peripheral and central regions of the liver

and plotted corresponding SNR measurements within these ROI for all TEs (Fig. 5b). SNR from the peripheral regions were typically more than double that of the SNR from the central regions for each volunteer. For the six volunteer studies, we calculated the measured R2* values resulting when truncating from SNR=0 to SNR=20, in both of the peripheral and central regions of liver parenchyma. At SNR truncation thresholds of 0, 7, 14, and 20, R2* values for both regions (across all volunteers) are plotted in Fig. 5c. For the peripheral region of liver parenchyma (higher SNR region due to coil proximity), R2* values from all three methods remained relatively constant at all thresholds and were not statistically different ($p>0.05$). In the central region, *Method C (VoxelOBC)* produced significantly different R2* values than both alternative approaches; however, these differences tended to be reduced with increasing truncation threshold.

Discussion

We compared three different approaches to improve R2* measurement accuracy in the setting of low SNR and rapid transverse signal decay. In phantoms, *ex vivo* animal model, and normal volunteer studies *Method C* (OBC reconstruction with rigorous SNR calculations for voxel-wise data truncation) consistently provided accurate R2* measurement. For all approaches, truncation proved to be an effective method to reduce R2* measurement error. OBC reconstructed data required less truncation compared to RSS data which required truncation at higher SNR thresholds. However, in practice, the SNR threshold that provides the minimum error may be unknown. With no *a priori* knowledge of the optimal threshold, *Method C* is particularly superior to the alternative approaches given the reduced requirement for data truncation.

Our phantom and animal model studies provided a range of R2* values such that we could compare signals and images reconstructed using both RSS and OBC combination methods. When attempting to characterize high R2* values in low SNR settings within a limited time echo range (high intrinsic R2*, low FA or later TEs), RSS signals were greatly impacted by noise bias due to the intrinsic limitations of this multichannel data combination technique. With the use of individual coil-sensitivity profiles, the OBC approach allowed a near-optimal combination of multi-coil signals even at low SNR, reducing the effects of noise on signal data. Conversely, both the RSS and the OBC methods produced near-optimal data for high SNR settings (low intrinsic R2*, higher FA or earlier TEs).

Within a given echo time range, the accuracy for R2* estimations was shown to be affected by the intrinsic R2* value, SNR level, and chosen reconstruction method. Mean VAE for R2* estimations in both phantom and animal studies decreased with increasing SNR level, decreasing R2* value, and use of the OBC reconstruction method. At a higher FA (increased SNR level), greater signal was available at each TE permitting a greater number of TE to be included in the fitting procedure for improved R2* estimation. At lower R2* values within a limited echo time range, signal decayed to the noise floor at a much slower rate similarly permitting a greater number TEs to be included without being negatively impacted by noise bias. OBC reconstruction demonstrated greater resistance to noise bias at later TEs and, therefore, superior R2* estimates. Truncation was quite effective for improving R2* measurement accuracy for the RSS combination approaches, particularly in low SNR settings when attempting to characterize high R2* values. However, appropriate SNR-based truncation requires reliable SNR measurements. The major drawbacks of the conventional SNR measurement method (shown in Equ [1a]) include: 1) the noise estimation can be inaccurate due to spatially variant noise characteristics; 2) SNRs in low SNR TEs are overestimated due to the overestimated signal strength from noise bias. In a high SNR setting, the standard deviation of the background is related to the standard deviation of signal by a constant factor. This relationship does not hold for low SNR settings (21).

Taking into account spatially variant noise characteristics, voxel-wise SNR estimates for RSS reconstructed images (shown in Equ [2]) were subjected to magnitude correction for bias removal and can be accurate. However, it has been shown in our phantom studies that this method does not achieve complete noise removal within very low SNR settings. The OBC approach allowed a near-optimal combination of multi-coil signals even at low SNR, reducing the effects of noise on signal data. Therefore, voxel-wise SNR estimates of OBC reconstructed images (shown in Equ [3]) were accurately reflected in the low SNR TEs. In general, voxel-wise SNR measurements (used for truncation with *Methods B* and *C*) produced less R2* estimation error than SNR measurements that assumed globally homogeneous noise characteristics (*Method A*). OBC reconstruction (used in *Method C*) provided better image quality than RSS reconstruction (used in *Method A* and *B*) at later TEs, thereby reducing the effect of noise bias for better R2* measurement. It should also be noted that in common practice, the anticipated range of R2* values within organ(s) of interest may be known *a priori* such that the chosen imaging protocol could use an appropriately limited echo range to attempt to avoid noise bias. Under these settings the intrinsic R2* value may have less of an impact upon the R2* measurement. Given the potential for a quite wide range R2* values (within or between individuals), optimal limiting of the echo time range may be critical to produce accurate R2* estimations. Sub-optimal limiting of the echo time range can reduce efficiency for MGRE-based R2* measurements leading to the inclusion of excessively few TEs for mono-exponential fitting; conversely, too wide of an echo time range produces low SNR images at later TEs (biased by noise) also leading to greater R2* estimation error. Our proposed methods were shown to improve R2* measurement while allowing flexible selection of echo time range (truncation based upon quantified SNR levels).

Volunteer images provided high SNR in peripheral regions and relatively low SNR in central regions due to penetration characteristics and alignment of the receivers (27). The number of channels (coils elements) used during our MGRE R2* measurements can strongly influence the noise bias level in the RSS images. The larger number of coil elements used for our volunteer studies (compared to our phantom and animal model studies) may have potentially resulted in a larger noise bias (17), increasing the noise bias dependent differences between RSS and OBC reconstruction methods. Therefore, R2* maps derived from these images were highly dependent upon the image reconstruction method. In healthy volunteers R2* within the liver parenchyma should be relatively homogenous provided adequate field shim (28,29,30). However, due to spatial SNR variations, noise biases can lead to highly heterogeneous R2* measurements with striking differences between R2* values measured within peripheral and central regions. In peripheral regions with relatively high SNR, RSS and OBC reconstructions were both nearly optimal. Within these peripheral regions R2* values for *Method A*, *Method B*, and *Method C* were not significantly different at each selected threshold. However, within the central region with low SNR, RSS images had a relatively high noise floor at later TEs, and therefore resulting RSS R2* values were likely to have been underestimated. OBC reconstruction had a lower noise floor at later TEs which should have provided superior R2* estimates. As expected, R2* estimates from RSS reconstruction were altered by truncation. At low SNR thresholds (thresholds=0-7), R2* estimates from RSS reconstructions (*Method A* and *B*) were small in comparison with R2* estimates from OBC reconstruction (*Method C*). However, the R2* values measured with these three comparison methods seemed to begin to converge at higher SNR truncation thresholds (reducing differences between R2* measured with OBC and RSS approaches as threshold was increased). While a “reference-standard” R2* measurement was not possible for these normal volunteer studies, our results suggest superior accuracy for *Method C* (*VoxelOBC*) given a) the consistently greater similarity between peripheral and central ROI liver R2* measurements for *Method C* and b)

convergence of *Methods A* and *B* R2* measurements toward *Method C* R2* estimates as truncation thresholds were increased.

Our study had several limitations. We investigated these R2* quantification approaches using only a finite, limited number of R2* values and SNR levels. Additionally, while we have provided data demonstrating that truncation can give rise to more accurate R2* measurements, we have yet to develop numerical methods to determine an optimal threshold *a priori* under different conditions. While computationally demanding, one possible approach to determine an optimal threshold would be to iteratively compute R2* values while using increasingly lower truncation thresholds. Lowering truncation thresholds (including fewer of the later TE) should progressively reduce noise bias leading to the calculation of longer R2* values; one could anticipate that at an optimal truncation level (or range of truncation levels) the calculated R2* level should remain relatively constant or perhaps achieve a local maximum. However, while such an approach may in principle permit effective identification of a near optimal truncation threshold, this procedure would be computationally intensive such that it may not be applicable for routine clinical use. Further investigation into efficient automated methods to determine these optimal thresholds (under differing conditions) is clearly warranted. A number of different noise bias correction methods have been proposed to correct magnitude images (12,13,14); while these methods have primarily been proposed for single coil images, these could readily be modified to account for non-central chi distributions within RSS combined images. These could each prove similarly advantageous methods to improve the accuracy of R2* methods. Future comprehensive studies should investigate and compare the strengths and weaknesses of these methods for R2* measurements. Additionally, the current study did not investigate the impact of specific coil array geometries and perhaps even more importantly the impact of imaging acceleration techniques (31,32). Finally, our studies considered only a mono-exponential decay model; future studies could investigate the utility of these methods for the estimation of bi-exponential decay components as recently described for fat quantification (33).

Conclusion

Our studies confirmed that data truncation based upon rigorous voxel-wise SNR estimates can reduce R2* measurement error in the setting of low SNR with fast signal decay. However, when optimal SNR truncation thresholds are unknown, the OBC method can provide optimal R2* measurement given its minimal truncation requirements.

Acknowledgments

The authors wish to thank Peter Kellman (Laboratory of Cardiac Energetics, National Heart, Lung and Blood Institute, National Institutes of Health, DHHS, Bethesda, MD, USA) for his essential advice on different SNR measurement methods. This publication was made possible in part by Grant Number CA134719 from the National Cancer Institute. Its contents are solely the responsibility of the authors and do not necessarily represent the official view of the NCI or NIH.

References

1. He T, Gatehouse PD, Kirk P, Mohiaddin RH, Pennell DJ, Firmin DN. Myocardial T*2 measurement in iron-overloaded thalassemia: an ex vivo study to investigate optimal methods of quantification. Magn Reson Med 2008;60:350–356. [PubMed: 18666131]
2. He T, Gatehouse PD, Kirk P, Mohiaddin RH, Pennell DJ, Firmin DN. Myocardial T2* measurements in iron-overloaded thalassemia: An in vivo study to investigate optimal methods of quantification. Magn Reson Med 2008;60:1082–1089. [PubMed: 18956471]

3. Wood JC, Enriquez C, Ghugre N, Tyzka JM, Carson S, Nelson MD, Coates TD. MRI R2 and R2* mapping accurately estimates hepatic iron concentration in transfusion-dependent thalassemia and sickle cell disease patients. Blood 2005 August 15;106(4):1460–1465. [PubMed: 15860670]
4. Virtanen JM, Komu ME, Parkokola RK. Quantitative liver iron measurement by magnetic resonance imaging: in vitro andn in vivo assessment of the liver muscle signal intensity and the R2* methods. Magn Reson Imaging 2008;26:1175–82. [PubMed: 18524528]
5. Gudbjartsson H, Patz S. The Rician Distribution of Noisy MRI Data. Magn Reson Med 1995;34:910–914. [PubMed: 8598820]
6. Dietrich O, Raya JG, Reiser MF. Magnetic resonance noise measurements and signal-quantization effects at very low noise levels. Magn Reson Med 2008;60:1477–1487. [PubMed: 19025912]
7. Graves MJ, Emmens D, Lejay H, Hariharan H, Polzin J, Lomas DJ. T2 and T2* quantification using optimal B1-image reconstruction for multcoil arrays. J Magn Reson Imaging 2008;28:278–281. [PubMed: 18581394]
8. Miller AJ, Joseph PM. The use of power images to perform quantitative analysis on low SNR MR images. Magn Reson Imaging 1993;11:1051–1056. [PubMed: 8231670]
9. Gambarota G, Cairns BE, Berde CB, Mulkern RV. Osmotic effects on the T2 relaxation decay of in vivo muscle. Magn Reson Med 2001;46:592–599. [PubMed: 11550254]
10. Ghugre NR, Enriquez CM, Coates TD, Nelson MD, Wood JC. Improved R2* measurements in myocardial iron overload. J Magn Reson Imaging 2006;23:9–16. [PubMed: 16329085]
11. Carneiro AAO, Vilela GR, de Araujo DB, Baffa O. MRI relaxometry: methods and applications. Braz J Phys 2006;36:9–15.
12. Dietrich O, Heiland S, Sartor K. Noise correction for the exact determination of apparent diffusion coefficients at low SNR. Magn Reson Med 2001;45:448–53. [PubMed: 11241703]
13. McGibney G, Smith MR. An unbiased signal-to-noise ratio measure for magnetic resonance images. Med Phys 1993;20:1077–1078. [PubMed: 8413015]
14. Henkelman RM. Measurement of signal intensities in the presence of noise in MR images. Med Phys 1985;12:232–233. [PubMed: 4000083]
15. Westwood M, Anderson LJ, Firmin DN, Gatehouse PD, Charrier CC, Wonke B, Pennell DJ. A single breath-hold multiecho T2* cardiovascular magnetic resonance technique for diagnosis of myocardial iron overload. J Magn Reson Imaging 2003;18:33–39. [PubMed: 12815637]
16. Westwood MA, Anderson LJ, Firmin DN, Gatehouse PD, Lorenz CH, Wonke B, Pennell DJ. Interscanner reproducibility of cardiovascular magnetic resonance T2* measurements of tissue iron in thalassemia. J Magn Reson Imaging 2003;18:616–620. [PubMed: 14579406]
17. Kellman P, McVeigh ER. Image reconstruction in SNR units: a general method for SNR measurement. Magn Reson Med 2005;54:1439–1447. [PubMed: 16261576]
18. Roemer PB, Edelstein WA, Hayes CE, Souza SP, Mueller OM. The NMR phased array. Magn Reson Med 1990;16:192–225. [PubMed: 2266841]
19. Babacan, SD.; Yin, X.; Larson, AC.; Katsaggelos, AG. Combination of MR surface coil images using weighted constrained least squares. Proceedings to IEEE International Conf. on Imaging Processing (ICIP'08); San Diego, USA. 2008. p. 2236-2239.
20. Gilbert G, Simard D, Beaudoin G. Impact of an improved combination of signals from array coils in diffusion tensor imaging. IEEE Trans Med Imaging 2007;26:1428–1436. [PubMed: 18041258]
21. Gilbert G. Measurement of signal-to-noise ratios in sum-of-squares MR images. J Magn Reson Imaging 2007;26:1678. [PubMed: 18059007]
22. Dietrich O, Raya JG, Reeder SB, Reiser MF, Schoenberg SO. Measurement of signal-to-noise ratios in MR images: influence of multichannel coils, parallel imaging, and reconstruction filters. J Magn Reson Imaging 2007;26:375–385. [PubMed: 17622966]
23. Constantinides CD, Atalar E, McVeigh ER. Signal-to-noise measurements in magnitude images from NMR phased arrays. Magn Reson Med 1997;38:852–857. [PubMed: 9358462]
24. Walsh DO, Gmitro AF, Marcellin MW. Adaptive reconstruction of phased array MR imagery. Magn Reson Med 2000;43:682–690. [PubMed: 10800033]
25. Woodcock RJ Jr, Short J, Do HM, Jensen ME, Kallmes DF. Imaging of acute subarachnoid hemorrhage with a fluid-attenuated inversion recovery sequence in an animal model: comparison

with non-contrast-enhanced CT. AJNR Am J Neuroradiol 2001;22(9):1698–703. [PubMed: 11673164]

26. Rhee TK, Larson AC, Prasad PV, Santos E, Sato KT, Salem R, Deng J, Paunesku T, Woloschak GE, Mulcahy MF, Li D, Omary RA. Feasibility of blood oxygenation level-dependent MR imaging to monitor hepatic transcatheter arterial embolization in rabbits. J Vasc Interv Radiol 2005;16(11):1523–8. [PubMed: 16319161]
27. Hardy CJ, Cline HE, Giaquinto RO, Niendorf T, Grant AK, Sodickson DK. 32-element receiver-coil array for cardiac imaging. Magn Reson Med 2006;55:1142–1149. [PubMed: 16596635]
28. Beaumont M, Odame I, Babyn PS, Vidarsson L, Kirby-Allen M, Cheng HL. Accurate liver T2 measurement of iron overload: a simulations investigation and in vivo study. J Magn Reson Imaging 2009;30:313–20. [PubMed: 19629985]
29. Positano V, Salani B, Pepe A, Santarelli MF, De Marchi D, Ramazzotti A, Favilli B, Cracolici E, Midiri M, Cianciulli P, Lombardi M, Landini L. Improved T2* assessment in liver iron overload by magnetic resonance imaging. Magn Reson Imaging 2009;27:188–97. [PubMed: 18667287]
30. Maris TG, Papakonstantinou O, Chatzimanoli V, Papadakis A, Pagonidis K, Papanikolaou N, Karantanas A, Gourtsoyiannis N. Myocardial and liver iron status using a fast T*2 quantitative MRI (T*2qMRI) technique. Magn Reson Med 2007;57:742–53. [PubMed: 17390359]
31. Blaimer M, Breuer F, Mueller M, Heidemann RM, Griswold MA, Jacob PM. SMASH, SENSE, PILS, GRAPPA how to choose the optimal method. Top Magn Reson Imaging 2004;15:223–236. [PubMed: 15548953]
32. Winkelmann S, Schaeffter T, Weiss S. Simultaneous imaging and R2* mapping using a radial multi-gradient-echo (rMGE) sequence. J Magn Reson Imaging 2006;24:939–944. [PubMed: 16958064]
33. O'Regan DP, Callaghan MF, Wylezinska-Arridge M, Fitzpatrick J, Naoumova RP, Hajnal JV, Schmitz SA. Liver fat content and T2*: simultaneous measurement by using breath-hold multiecho MR imaging at 3.0 T—feasibility. Radiology 2008 May;247(2):550–557. [PubMed: 18349314]

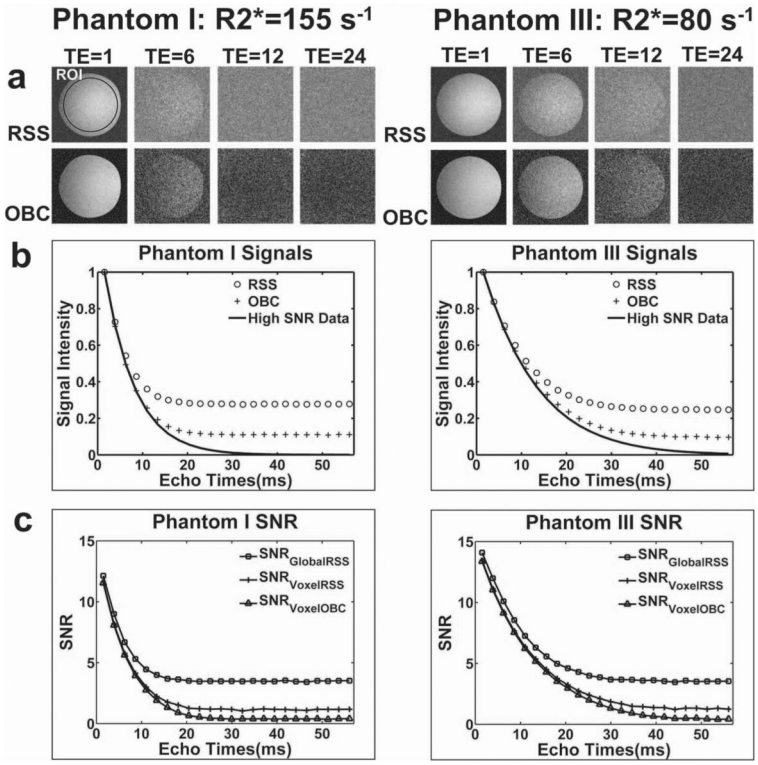

Figure 1.

R2* Phantom Studies. (**a**) RSS and OBC reconstructed images for *Phantom I* (R2*=155 s^{-1}) and *Phantom III* (R2*=80 s^{-1}) at TE=1.51ms, 13.36ms, 27.58ms, 56.02ms (echoes 1, 6, 12, and 24). Representative ROI drawn for comparisons of signal intensities and SNR measurements is shown within the RSS reconstructed image at TE=1. (**b**) Mean signal decay within RSS, OBC, and high SNR data for *Phantom I* and *Phantom III* image series. (**c**) SNR measurements at all TEs for RSS and OBC reconstructions: $SNR_{GlobalRSS}$, $SNR_{VoxelRSS}$, and $SNR_{VoxelOBC}$. Reconstructed images and signal plots show that RSS signal decays more rapidly to the noise floor than OBC reconstructed images. SNR measurements revealed the stronger impact of noise bias upon RSS reconstructions (*GlobalRSS and VoxelRSS*) as compared to OBC reconstruction *(VoxelOBC)*. Global SNR assessment for RSS reconstructions demonstrate greater impact of noise bias than the voxel-wise SNR assessments ($SNR_{GlobalRSS}$ vs. $SNR_{VoxelRSS}$).

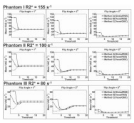

Figure 2.

Truncation Dependent Voxel-wise Absolute Error (VAE) for R2* Phantoms. For FA=1°, 2°, and 5°, mean VAE at truncation thresholds from 0 to 20 are displayed for *Phantom I*, *II*, and *III*. Mean VAE was reduced with increasing FA (increasing SNR) and decreasing R2* value. Mean VAE curves approached their minimum value as the SNR truncation threshold was decreased; mean VAE increased with the use of increasingly higher truncation thresholds. Limited truncation was needed for *Method C (VoxelOBC)* method to achieve the minimum VAE levels. *Methods A (GlobalRSS)* and *B (VoxelRSS)* required data truncation at higher SNR thresholds to achieve minimum VAE. In general, *Method A* had the highest level of mean VAE while *Method C* achieved the lowest level of VAE.

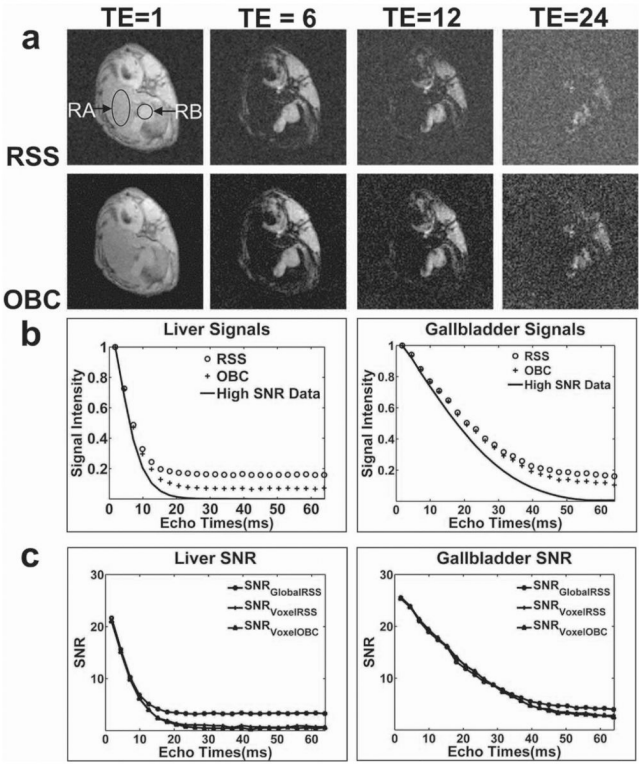

Figure 3.

Ex vivo Animal Model Studies. (**a**) RSS and OBC reconstructed echoes at TE=1.51ms, 13.36ms, 27.58ms, 56.02ms (echoes 1, 6, 12, and 24), with representative liver parenchyma and gallbladder ROIs (RA and RB respectively) drawn upon TE=1.51ms image. (**b**) Mean signal decay for RSS, OBC, and high SNR data within liver and gallbladder ROIs. (**c**) Global and voxel-wise SNR measurements for each reconstruction methods at all TEs. Images, and signal intensity plots each demonstrate that noise bias exerts a greater impact upon RSS reconstructed data than OBC reconstructed data. SNR measurements revealed the stronger impact of noise bias upon relative SNR measurement ($SNR_{GlobalRSS}$) as compared to absolute voxel-wise SNR measurements ($SNR_{VoxelRSS}$ *and* $SNR_{VoxelOBC}$). The R2* for liver parenchyma was much greater than the R2* of the gallbladder (reference standard R2* values were $160s^{-1}$ and $50s^{-1}$ respectively). Therefore, signal intensities and SNR measurements for the gallbladder were less affected by noise bias over the same range of TEs.

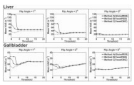

Figure 4.
Truncation Dependent Voxel-wise Absolute Error (VAE) for Animal Model R2* Measurements. For FA=1°, 2°, and 5°, mean VAE at truncation thresholds from 0 to 20 are shown for both liver and gallbladder ROIs. Similar to previous phantom studies, mean VAE decreased with increasing SNR and decreasing R2* value. To achieve the optimal VAE level, *Method C (VoxelOBC)* required little or no truncation, while *Method A(GlobalRSS)* and *B(VoxelRSS)* required a higher level of truncation. *Method A* had the highest level of mean VAE while *Method C* achieved the lowest VAE.

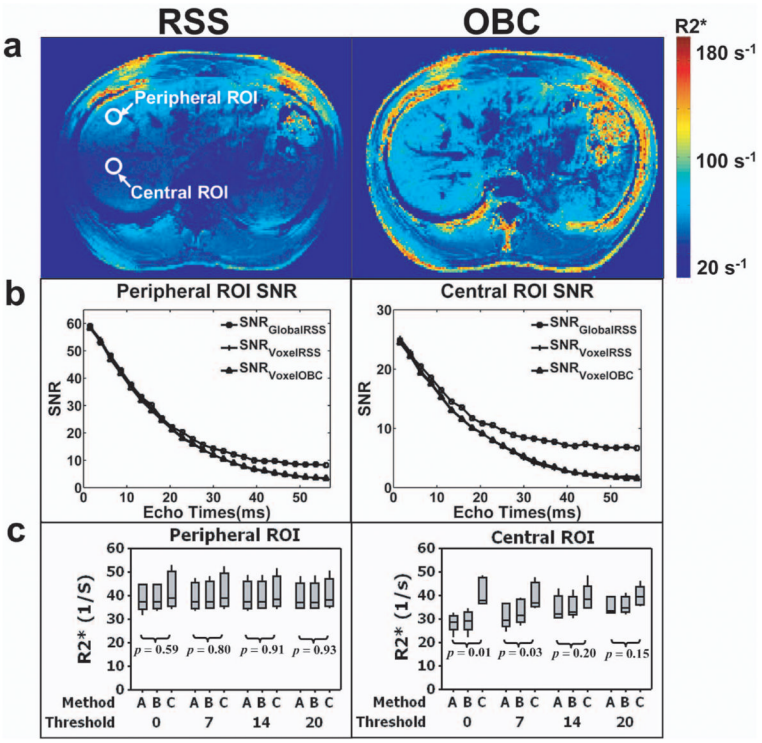

Figure 5.

Normal Volunteer Studies. (**a**) Axial orientation R2* maps for a single representative volunteer derived from 24 TEs of RSS and OBC reconstructed data at FA=20°. Representative ROIs from peripheral and central regions of liver parenchyma are shown on RSS reconstructed R2* map; (**b**) SNR plots for peripheral and central ROIs of liver parenchyma; (**c**) For six normal volunteer studies, boxplots depicting the mean R2* values from the peripheral and central ROIs shown to compare the three methods at truncation thresholds=0, 7, 14, and 20. Top and bottom of each boxplot represents the third (Q3, 75% of the values < Q3) and first quartile (Q1, 25% of the values < Q1) of the data values, respectively. The central bar within each box is the data median, and the upper and lower whiskers are the highest and lowest data values within the upper and lower limits (Upper limit=Q3 + 1.5×(Q3 - Q1); Lower limit=Q1-1.5×(Q3 - Q1)). Signals from the peripheral region of liver parenchyma have higher SNR than signals from the central region at all TEs. Boxplots demonstrate that the R2* values for *Methods A*, *B*, and *C* remained relatively constant in the peripheral region of the liver parenchyma for all thresholds ($p>0.05$). In the central region of liver parenchyma, *Method C (VoxelOBC)* produced significantly different R2* values than both alternative approaches; however, these differences tended to be reduced with increasing truncation threshold.

Table 1
Sequence Parameters For Phantom, Animal, and Volunteer Studies

	Phantom Studies	Animal Study	Volunteer Studies
TR (ms)	5000	1000	100 (liver)
TE (ms) 1^{st}/spacing/24^{th}	1.51/2.37/56	1.67/2.7/66.8	1.57/2.57/60.7
Flip Angle(degree)	1, 2, 5, 10	1, 2, 5, 10	20
Bandwidth (Hz/pixel)	1302	640	640
Field of View (mm)	250	250	350-400
Matrix	256×256	192×132	192×128
Coil Channels	8	8	32
GS Averages	32	32	0